5th International Conference on Experimental Fluid Mechanics ICEFM 2018 Munich
Munich, Germany, July 2-4, 2018

Large scale motions behind a spinning rough sphere

Zhuoyue Li, Nan Gao*

Dalian University of Technology, School of Aeronautics, Dalian, China

* gaonan@dlut.edu.cn

Abstract

Aerodynamic forces on a rotating golf ball were measured in a water tunnel for a Reynolds number of Re_D= 8000 at a spinning ratio V_s/U_o (the surface velocity over the freestream velocity) between 0 and 6.0. The flow fields downstream of a spinning sphere were also measured using a time-resolved stereoscopic PIV system with field-of-views perpendicular to the incoming flow to capture the three velocity components.There appeared to be several critical spinning ratios at $V_s/U_o \approx$ 0.75, 2.0 and 3.0. Both lift and drag increased quickly for $V_s/U_o \lesssim 0.75$; there was a sudden drop in lift at $V_s/U_o \approx$ 0.75; lift increased quickly while drag increased slowly for $1.0 \lesssim V_s/U_o \lesssim 2.0$; both lift and drag plateaued for $2.0 \lesssim V_s/U_o \lesssim 3.0$; lift increased while drag decreased for large spinning ratios $3.0 \lesssim V_s/U_o \lesssim 6.0$. Flow measurements suggested the lift increase was associated with a downwash downstream of spinning ball. It leaded to a pair of counter-rotating vortices that caused increases in drag, similar to the induced drag on a finite-span wing. Boundary layer transition occurred on retreating side at a large spinning ratio $3.0 \lesssim V_s/U_o \lesssim 6.0$, the strength of the trailing vortex pair got weaker in this situation and drag increased thus became smaller again.

1 Introduction

The spinning motion of a solid particle translating in fluid generates lift force, which is referred to as the Magnus effect. This phenomenon was studied using experimental methods Tsuji Y (1985); Kray et al. (2012); Kim et al. (2007, 2014) and numerical simulations Muto et al. (2011, 2012); Li et al. (2017); Citro et al. (2017); Zhou and Fan (2015). Recent investigations by Kim et al. (2007, 2014) and Muto et al. (2011) found that the lift and drag forces on the particle undergo significant changes when the status of the boundary layer over the advancing side of the particle transitioned to a turbulent state , there could be a negative lift force generated. In their case, the transition occurred at a spinning ratio V_s/U_o (ratio of the surface velocity over the freestream velocity) of 0.75 to 1.0 and a Reynolds number close to the transitional Reynolds number.

The critical Reynolds number at which the boundary layer transitioned to a turbulent state was much smaller for a rough sphere (e.g. a golf ball) than that for a smooth sphere. The influence of dimple depth on the transition can be found in Chowdhury et al. (2016). Aoki et al. (2010) studied the drag and the separation point movement of a golf ball for spinning ratio $V_s/U_o \leq 0.2$ using both experiment and large eddy simulation (LES). Li et al. (2017) studied the aerodynamics forces and the flow structures downstream of a spinning golf ball using LES for a spinning ratio of $V_s/U_o = 0.1$. They also found inverse Magnus effect occurred at the critical Reynolds number regime, similar to the flow around a smooth sphere. Meanwhile they found that flow structures downstream of the sphere became more regular due to the spinning motion, and the lateral forces on the sphere also became stabilized. Fig. 1 shows typically flow structures downstream of a spinning sphere.

Until now, the existing investigations focused on the spinning sphere with a modest spinning ratio $V_s/U_o \leq 2.0$. It is expected that as V_s/U_o increases, the boundary layer on the retreating side could also transition to a turbulent state. The relation between the aerodynamic force and the flow structures was not studied before, therefore the current investigation will focus on lift and drag forces and coherent flow structures over a large range of spinning ratios $0 \leq V_s/U_o \leq 6.0$. The experimental methodologies will be presented in the next section, followed by the results and discussion and concluding remarks.

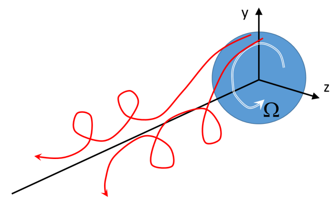

Figure 1: Schematics of flow over a spinning sphere

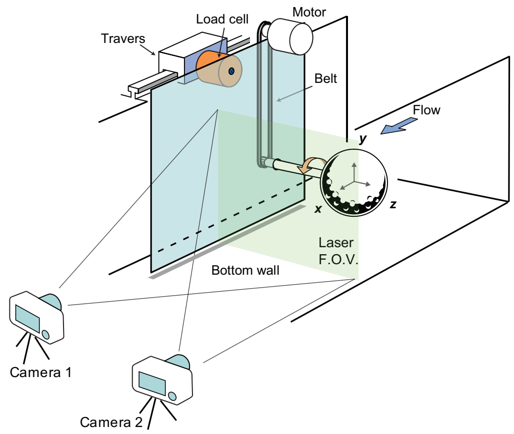

Figure 2: Schematics of the experimental facility.

2 Experimental Methodology

Measurements were performed in a recirculation water tunnel with a test section of $20\,cm \times 30\,cm \times 60\,cm$ (width, height, length). A two dimensional contraction section was used with a contraction ratio of 6.0. A pump with a $3\,kW$ motor was used to deliver the water. The maximum velocity was $0.4\,m/s$. A $5\,cm$ long, $4\,mm$ diameter honeycomb flow straightener was used in the delivery plenum upstream of the contraction section. The turbulence level in the test section was less than 1.0%. The water velocity in the test section can be varied manually by adjusting the motor speed using a frequency drive.

The test section was shown in Fig. 2. A golf ball ($D = 40$mm diameter, dimple diameter $0.09D$, dimple depth $0.005D$) was hold in the center of the test section by a $0.15D$ diameter steel support rod. The rod was connected to a stepper motor using a bell and pulley system. The motor and the rod were both mounted on a $5\,mm$ thick plexiglas plate that was connected to a traversing mechanism through a two-component load cell to measure the changes in the lift and drag forces. The whole assembly can be traversed for a distance of $20\,cm$ to measure the flow velocity at $x/D = 0.5$ to 5.0 for a $\Delta x/D = 0.5$. The measurements were performed for a free-stream velocity of $U_o = 0.22\,m/s$, corresponds to a Reynolds number of $Re_D = 8720$ based on the ball diameter. The spinning ratio $V_s/U_o = \omega D/2U_o$ can be changed form $0 \sim 6.0$.

A LaVision stereoscopic particle image velocimetry system was used to measure the flow velocities on planes perpendicular to the freestream velocity. Water was seeded using silver coated hollow glass spheres with a nominal diameter of $10\,\mu m$ (Dantec S-HGS-10). A 200mJ dual head Nd-YAG pulse laser system (Litron Nano) was used to illuminate the tracer particles. A LaVision supplied Highspeedstar camera with a 768 * 512 pixel resolution was used to capture the images. The time interval between two exposures was $1500\mu s$. The LaVision supplied DaVis 8.1 software package was used for image acquisition and post-processing. Vectors were computed using image cross correlations with 24 * 24 and 16 * 16 pixel interrogation windows and a 50% overlap in the first and second passes, respectively. A total of 2000 snapshots were acquired at a rate of 50 Hz. According to the method in Wieneke (2015), the uncertainty of PIV velocity fields were less than $\pm 2\%$ for a 95% confidence level. Signals from the load cell were acquired using a computer and a NI-6014 DAQ card at a sample rate of 1024Hz and a sampling time of 180 seconds. Five independent measurements of forces were taken for each spinning ratio.

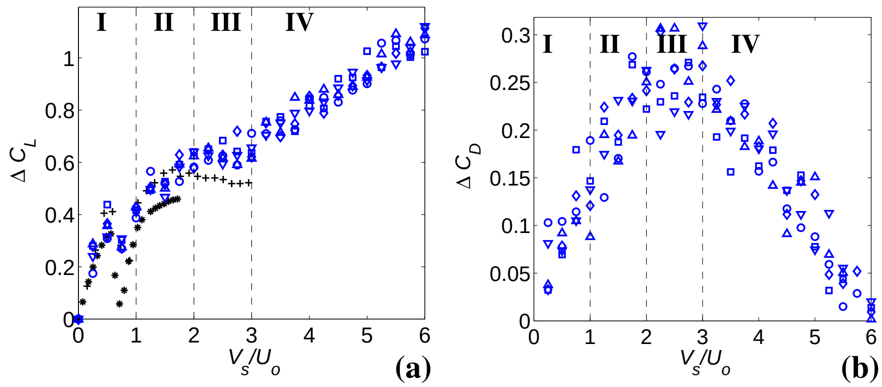

Figure 3: Distributions of changes of (a) lift and (b) drag by rotating speed of V_s/U_o, where $V_s = \omega D/2$. $C_L = 0$ and $C_D \approx 0.4$ for case with $V_s = 0$ according to refs. Aoki et al. (2010); Chowdhury et al. (2016). Five independent measurements were taken for each spinning ratio. Lift reported in refs. + Kray et al. (2012) and * Kim et al. (2007, 2014) were also shown for comparisons.

3 Results and Discussions

The time-averaged increases in the lift and drag forces (ΔC_L and ΔC_D) on the sphere for spinning ratio $V_s/U_o = 0$ to 6.0 are shown in Fig. 3. The changes in drag and lift with V_s/U_o suggested that there were four distinct flow regimes. $C_L = 0$ when $V_s/U_o = 0$, therefore $C_L = \Delta C_L$ in the current investigation. In the first regime $V_s/U_o \lesssim 0.75$, both lift and drag increased quickly, than there was a sudden drop in lift at $V_s/U_o \approx 0.75$ where previous investigation observed large decreases in lift, in agreement with literature data in Kray et al. (2012); Kim et al. (2007, 2014). In the second regime $1.0 \lesssim V_s/U_o \lesssim 2.0$, drag increased quickly but lift increased at a rate slower than region I; both lift and drag plateaued in regime III ($2.0 \lesssim V_s/U_o \lesssim 3.0$), the drag coefficient increased by over 60% as $C_D \approx 0.4$ according to refs. Aoki et al. (2010); Chowdhury et al. (2016). In the regime IV ($3.0 \lesssim V_s/U_o \lesssim 6.0$), lift increased with V_s/U_o while drag decreased quickly to $\Delta C_L \approx 0$ at $V_s/U_o = 6.0$.

The time-averaged velocity vectors and streamwise vorticity ω_x^* measured downstream of the sphere at $x/H = 0.5$ to 4.5 are shown in Fig. 4. In the flow without spinning ($V_s/U_o = 0$), structures firstly appeared around the sphere like a ring at $x/H = 0.5$, then became to a pair of counter rotating vortices at $x/H = 1.5$ and finally became incoherent at $x/H = 4.5$. When the sphere spinning with a ratio of $V_s/U_o = 0.5$, a pair of counter rotating vortices symmetrical about the xy plane appeared at $x/H = 0.5$ and gradually gone weaken with x/H, similar to the wing-tip vortices. The downwash of the spinning motion increased the left while the vortex pair increased the drag. When the spinning ratio increased, the strength of the downwash vectors seemed to increase from $V_s/U_o = 1.0$ to 6.0, but the strength of the vortex pair appeared to increase to $V_s/U_o = 1.0$ and 3.0 then seemed to decrease when V_s/U_o further increased to 6.0.

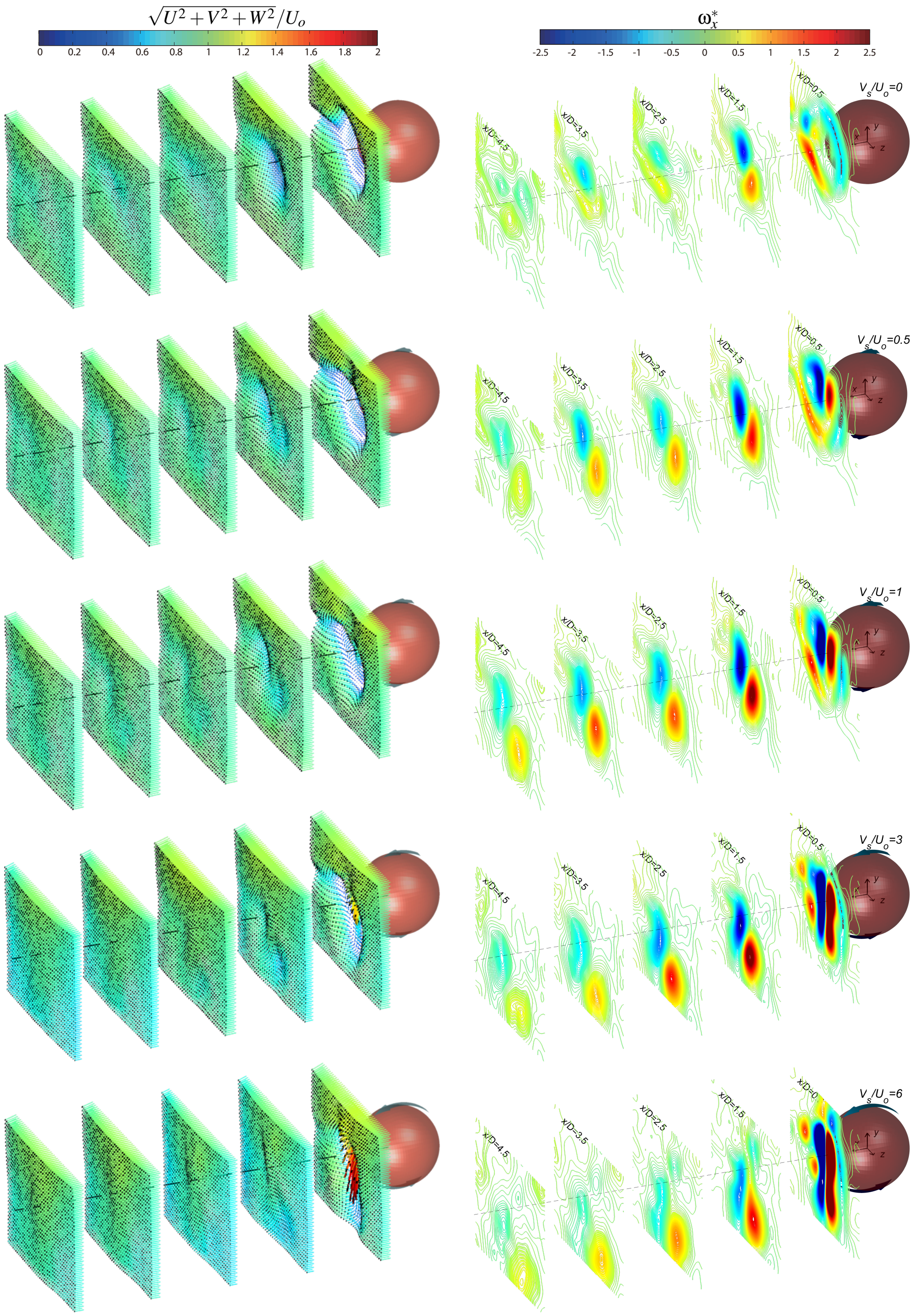

Figure 4: Distributions of (left) mean velocity vectors and (right) mean vorticity $\omega_x^* = \overline{\omega_x} D/U_o$ at x/H =0.5 to 4.5 at a $\Delta x/H$ =0.5 for spinning ratios of V_s/U_o = 0,0.5, 1, 3 and 6 (from top to bottom). Incoming flow is from right to left.

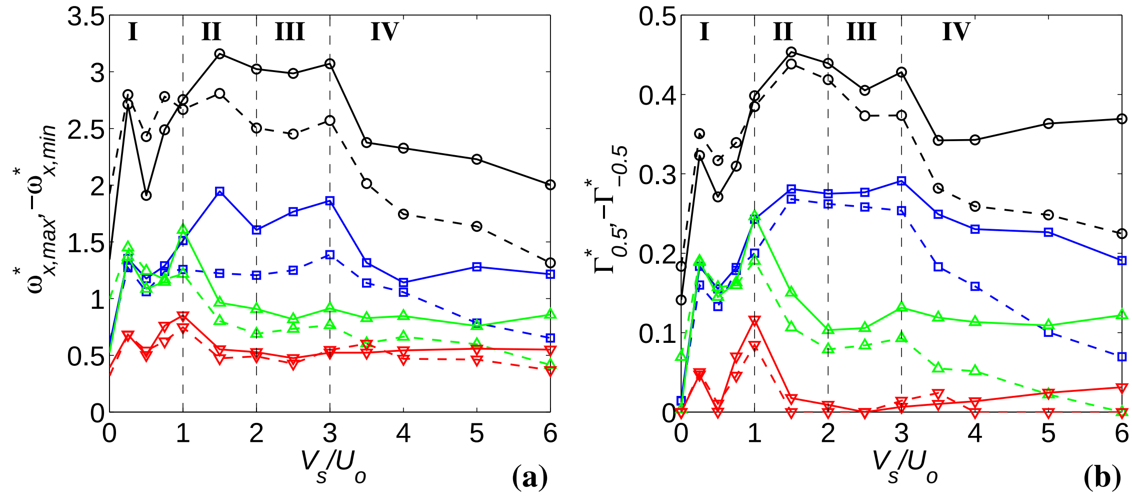

Figure 5: Distributions of the **(a)** maximum vorticity $\omega^*_{x,max}$ (solid line) and minimum vorticity $-\omega^*_{x,min}$ (dashed line) and **(b)** the vorticity circulation along the line $\omega^*_x = 0.5$ as $\Gamma^*_{0.5}$ (solid line) and $\omega^*_x = -0.5$ as $-\Gamma^*_{-0.5}$ (dashed line). Measuring plane was ◯x/H =1.5, □2.5 , △3.5 and ▽4.5.

To make a detailed analysis to the influence of the spinning ratio, the strength of the vortex pair downstream of the sphere were described using maximum and minimum vorticity $\omega^*_{x,max}, -\omega^*_{x,min}$ in Fig. 5 (a) and vorticity circulation $\Gamma^*_{0.5}, -\Gamma^*_{-0.5}$ in Fig. 5 (b). We noticed these two variables showed similar behaviours with the spinning ratio. In regime I $V_s/U_o < 1$, the strength of the vortex pair first increased than sudden dropped at $V_s/U_o \approx 0.5$. At place x/H =0.5 and 1.5, the strength continues to increased in regime II, then plateaued in regime III and stared to decrease with spinning ratio got to regime IV $V_s/U_o > 3$. It is therefore reasonable to conjecture that the drag decreases in region IV were associated with the breaking down of the trailing vortex pair.

4 Concluding Remarks

Lift and drag forces on a rotating golf ball were measured in a water tunnel for a Reynolds number of Re_D= 8000 at a spinning ratio V_s/U_o of 0 to 6.0. The flow fields downstream of a spinning sphere were also measured using a time-resolved stereoscopic PIV system. There appeared to be four distinct flow regimes: in regime I both lift and drag increased quickly for spinning ratio $V_s/U_o \lesssim 0.5$; this was followed by a sudden drop in lift at $V_s/U_o \approx 0.75$; in regime II lift increased quickly while drag increased slowly for spinning ratio $0.75 \lesssim V_s/U_o \lesssim 2.0$; in regime III both lift and drag plateaued at $2.0 \lesssim V_s/U_o \lesssim 3.0$; in regime IV lift increased while drag decreased for a spinning ratio $3.0 \lesssim V_s/U_o \lesssim 6.0$. Flow measurements suggested down wash associated with the spinning motion caused the increase in the lift, as well as a pair of counter-rotating vortices which in turn caused increases in drag, the mechanism of drag increase was similar to the induced drag on a finite-span wing. It was conjectured that boundary layer transition occurred on retreating side at a large spinning ratio $3.0 \lesssim V_s/U_o \lesssim 6.0$, the strength of the trailing vortex pair appeared to be weaker in this situation and drag increased thus became smaller.

Acknowledgements

The research was funded by Natural Science Foundation of China (91752101,11572078) and 973 Plan (2014CB744100).

References

Aoki K, Muto K, and Okanaga H (2010) Aerodynamic characteristics and flow pattern of a golf ball with rotation. *Procedia Engineering* 2:2431 – 2436. the Engineering of Sport 8 - Engineering Emotion

Chowdhury H, Loganathan B, Wang Y, Mustary I, and Alam F (2016) A study of dimple characteristics on golf ball drag. *Procedia Engineering* 147:87 – 91. the Engineering of SPORT 11

Citro V, Siconolfi L, Fabre D, Giannetti F, and Luchini P (2017) Stability and sensitivity analysis of the secondary instability in the sphere wake. *AIAA Journal* 55:1–8

Kim J, Choi H, Park H, and Yoo JY (2014) Inverse magnus effect on a rotating sphere: when and why. *Journal of Fluid Mechanics* 754

Kim J, Park H, Choi H, and Yoo J (2007) Inverse magnus effect on a rotating sphere. in *International symposium on turbulence and shear flow phenomena, TSFP-8*. AER2D

Kray T, Franke J, and Frank W (2012) Magnus effect on a rotating sphere at high reynolds numbers. *Journal of Wind Engineering and Industrial Aerodynamics* 110:1 – 9

Li J, Tsubokura M, and Tsunoda M (2017) Numerical investigation of the flow past a rotating golf ball and its comparison with a rotating smooth sphere. *Flow, Turbulence and Combustion* 99:837–864

Muto M, Tsubokura M, and Oshima N (2012) Negative magnus effect on a rotating sphere at around the critical reynolds number. *Physics of Fluids* 24:014102

Muto M, Watanabe H, Tsubokura M, and Oshima N (2011) Negative magnus effect on a rotating sphere at around the critical reynolds number. *Journal of Physics: Conference Series* 318:032021

Tsuji Y MO Morikawa Y (1985) Experimental measurement of the magnus force on a rotating sphere at low reynolds numbers. *Journal of Fluids Engineering* 107(4):484 – 488

Wieneke B (2015) PIV uncertainty quantification from correlation statistics. *Meas Sci Technol* 26:074002

Zhou Q and Fan LS (2015) Direct numerical simulation of low-reynolds-number flow past arrays of rotating spheres. *Journal of Fluid Mechanics* 765:396–423